TRC
Typhoon Science and Technology Research Center

YNU
Yokohama National University

Institute for Multidisciplinary Sciences
Yokohama National University

IWTRC 2023 YOKOHAMA

ABSTRACTS (KEYNOTES)

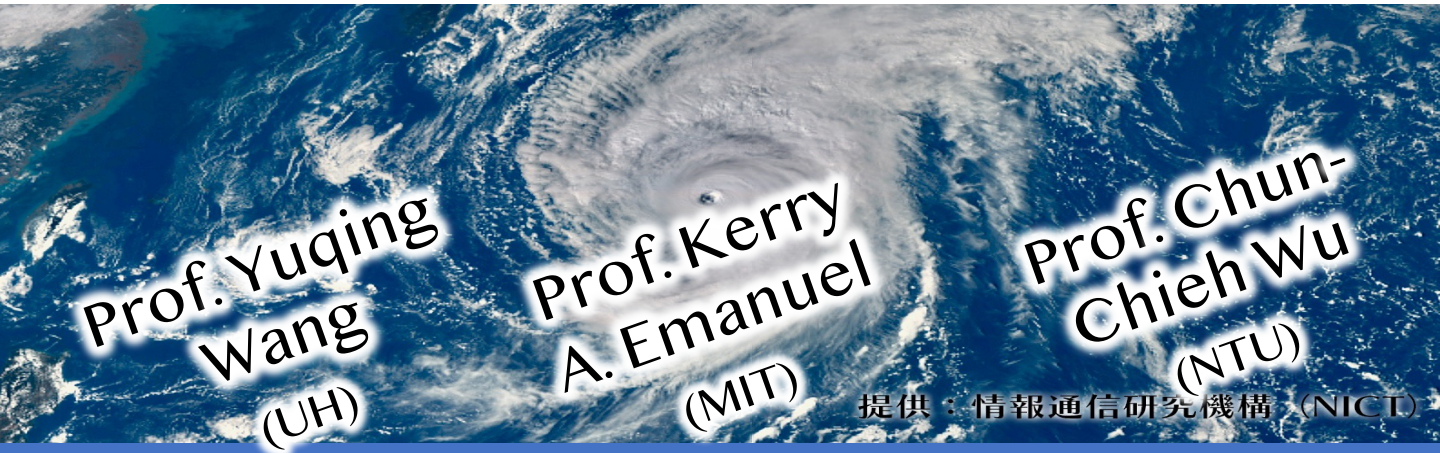

The 1st International Workshop of the Typhoon Science and Technology Research Center

November 8-9, 2023 on-site

Yokohama National University, Japan

https://trc.ynu.ac.jp/IWTRC/

Presented with the Support of

FUJITSU

MS&AD INSURANCE GROUP

The challenge of estimating long-term tropical cyclone risk

Kerry Emanuel
Massachusetts Institute of Technology, USA
emanuel@mit.edu

1. The nature of long-term natural hazard risk

Natural hazards cause enormous destruction and dislocation worldwide. Long-term records of such hazards show that their average annual loss (AAL, the total damage over the long record divided by the number of years in the record) tends to be dominated by "100-year events", those events with an annual probability of about 0.01. Societies are usually well adapted to events that are somewhat more frequent, while rarer events, though individually more destructive, are too infrequent to dominate the AAL. Large problems arise when, owing to climate change, events that used to be very rare become less so (e.g. 250-year events becoming 50-year events).

This presents two important problems for estimating long-term hazard risk. First, robust estimates of 100-year events require at least 1,000 years of data, which we almost never have. This requires us to "regionalize" risk… a 100-year event for a specific location maybe a 10-year event for a large enough region around it, and so we may be able to robustly estimate the latter. But translating regional risk to local risk requires us to assume homogeneity of risk over the region. This assumption is often dubious…e.g. earthquakes are concentrated along fault lines, heavy rains are often focused on topographic features, and storm surge magnitude depends sensitively on the local shape of the coast and the near-shore bathymetry.

The second problem, particular to meteorological hazards, is that, owing to climate change, historical statistics have largely ceased to be relevant to current risk. For this reason, it is imperative that risk be estimated from physics, including physics-based numerical models, rather than exclusively from historical statistics. Yet most extant decision making, including the pricing of insurance, continues to be modeled on inadequate and often irrelevant historical statistics. The estimation of risk it far too important to be left to statisticians and desperately requires input from scientists specializing in the physics and numerical modeling of the hazards.

2. Physical risk modeling

An obvious way to estimate long-term weather hazard risk under a changing climate is to employ global climate models. The numerical requirements, however, are daunting. Many weather hazards, including severe local storms, are not currently resolvable by climate models, and even well-resolved phenomena, such as large-scale blocking patterns – responsible for prolonged heat waves and droughts – are not handled particularly well by today's models. Even if they were, one would have to perform thousands of years of simulations to capture the rare events that dominate AAL, and do so with many different models to account for model errors and biases.

Phenomena unresolved by global models (e.g. severe local storms) must either be downscaled – by driving high-resolution local and/or regional models with the global model output, or predicted using statistical or AI-type algorithms applied to the global model fields. The latter technique is risky because the algorithms must be trained on past data that may not adequately reflect climate change. To take a concrete example, climate

change effects on severe convective storms are currently assessed by noting changes in large-scale correlates – e.g. wind shear and convective available potential energy – explicitly predicted by global climate models. Such assessments are not necessarily informed by a deep understanding of the physics underlying the changes in the large-scale correlates.

3. Tropical cyclone risk modeling

There is by now a large literature on the direct simulation of tropical cyclones by global models; see the review papers by Knutson et al. (2019, 2020). The global models used have horizontal grid spacing ranging from about 15 km to as much as 120 km. Many inferences have been made using such models in spite of the fact that even the finest resolution of these do not adequately resolve tropical cyclones. We know from observations, theory, and highly specialized tropical cyclone models (e.g. Rotunno et al. 2009) that the all-important eyewall has dimensions of order 10 km and requires grid-spacings of a few kilometers for numerical convergence. The more intense tropical cyclones have even more stringent resolution requirements. Consequently, assessments based directly on today's global climate models may prove to be ill-founded.

Alternatives to direct simulation of tropical cyclones by global models include deterministic and deterministic/statistical downscaling. In the first approach, fine-scale regional models are either embedded within the global model, providing two-way interaction, or driven offline by the global model output. In the second approach, statistics of the global fields (e.g. monthly mean thermodynamics and means and variances of winds) are used to drive simplified models of genesis, tracks and intensity.

In this paper, I will use the particular downscaling method developed by the author and his collaborators (Emanuel et al. 2008) to illustrate how appropriately constructed tropical cyclone downscaling from global reanalyses and climate models can be used to help estimate current and future risk from these storms. Broadly, the track model is a beta-and-advection model driven by time series of winds at two levels in the troposphere, synthesized from the global model or reanalysis daily winds such that the monthly means and covariances among the different wind components at the two levels are always correct, and that the power spectrum follows geostrophic turbulence scaling. The intensity model is the Coupled Hurricane Intensity Prediction System (CHIPS; Emanuel et al. 2004), an axisymmetric coupled ocean-atmosphere model phrased in a coordinate system for which the radial coordinate is the square root of the absolute angular momentum. This yields very high resolution (~ 1 km) in the all-important eyewall region while using relatively few computational models. Wind shear effects are parameterized such as to optimize real-time intensity forecasts (Emanuel and Rappaport 2000). The thermodynamic components, including the potential intensity and upper ocean thermal structure, are provided by monthly mean output of the climate model. Genesis is simulated by space-time random seeding of the global fields with weak proto-vortices. Most of these fail to develop, owing to having been placed in unsuitable large-scale environments; those that do are regarded as constituting the tropical cyclone climatology for the reanalysis or global model used to drive the algorithm. Random seeding has been shown to work well provided the seeds are weak enough (Emanuel 2022) and when applied to reanalyses, the algorithm produces realistic intensity probability distributions, track and genesis distributions, seasonal cycles, and ENSO-induced variability (e.g. Emanuel et al. 2008). That an independent seed climatology does not appear to be necessary is consistent with the results of Patricola et al. (2018) and Danso et al. (2022).

Tropical cyclone events generated using this or other downscaling methods can be used to drive hydrodynamic storm surge models (e.g. Lin et al. 2010) to assess surge risk, and rain associated with the tropical cyclones (Feldmann et al. 2019) can be used to drive hydraulic flood models (Bates et al. 2021) to assess tropical cyclone freshwater flood risk.

4. From physical hazards to long-term risk

Quantifying the statistics and physical characteristics of weather hazards is half the battle. The other half is turning hazard risk into economic and social risk and conveying those risks to those who need to know them. This second step is as unknown to most weather and climate scientists as the first step is to insurers, politicians, emergency managers, and other users of risk information. We need to educate a new generation of scientists who are well acquainted with both these endeavors.

To illustrate what can be done with sufficiently large sets of tropical cyclone events under a changing climate, we used the aforementioned technique to generate 6,200 tropical cyclone events that affect the eastern U.S., driven by output from each of 8 global climate models over each of the periods 1984-2014, and 2070-2100 under a middle-of-the-road greenhouse gas emissions scenario (SSP3-7.0). The total number of tracks was therefore close to 100,000. We then used these synthetic hurricane events to estimate damage to a large portfolio of insured property aggregated over 12,968 zip codes, assigning all the value in each zip code to the geographical centroid of that zip code. The fraction of total insured value (TIV) destroyed in each zip code was estimated by applying an idealized wind damage function (Emanuel et al. 2012) to the peak wind experienced during each hurricane event at each zip code centroid. The TIV of this portfolio is close to $2 trillion.

The annual exceedance probability of damage to this portfolio of insured property is shown in Figure 1; note that the damage is on a log scale.

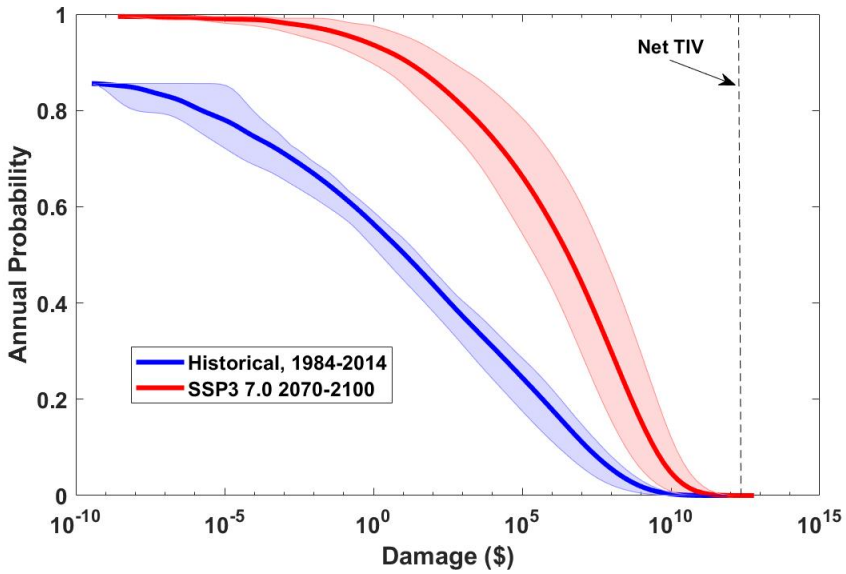

Fig. 1: Annual exceedance probability of damage exceeding the amount shown on the abscissa. The Total Insured Value (TIV) of this portfolio, shown by the vertical dashed line at right, is about $2 trillion. The solid curves show the multi-model means and the shading denotes the 5th and 95th quantiles among the 8 models. Blue is for the historical period and red is for the end of the 21st century.

The multi-model median annual damage, with an exceedance probability of 0.5, is only $12 for the historical period, showing high levels of adaptation to the climate of the past, but rises to $3.5 million by the end of this century, still a tiny fraction of the TIV.

Figure 2 shows the same data displayed a different way. On the ordinate we now have the exceedance probability multiplied by the corresponding damage itself, representing the loss density. The area under these curves gives the Average Annual Loss (AAL). The multi-model mean AAL for the historical period is $536 million, and for the end of the century is $4.1 billion. By comparing figures 1 and 2 it can readily be seen that the main contributions to the AAL are by exceedingly rare events, with average return periods of more than 450 years in the historical climate and more than 100 years in the climate of the end of this century. Note also the extremely large uncertainty in AAL, indicated by the spread among the climate models downscaled (red shading in figure).

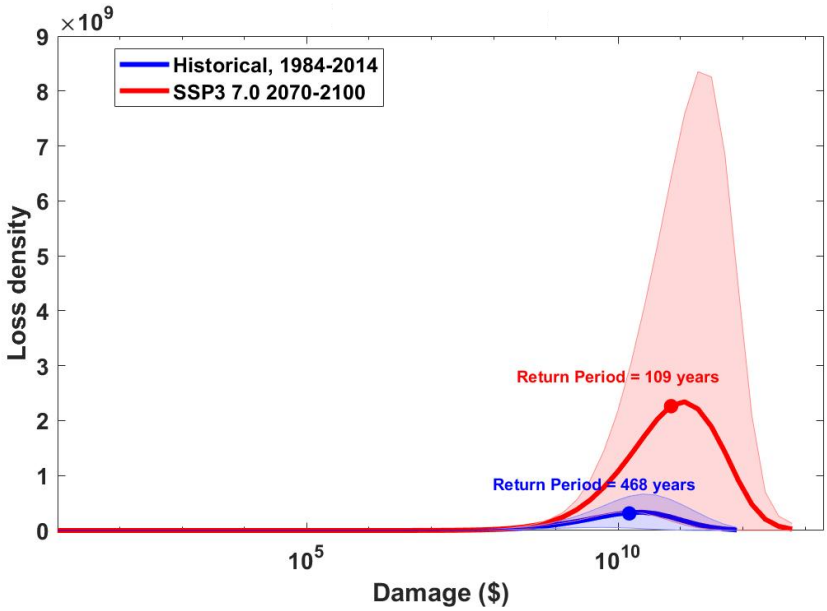

Fig. 2: Loss density ($) corresponding to Fig. 1, produced by multiplying the exceedance probability by the damage associated with it. The area under the curves is the average annual loss (AAL). The return periods of the main contributors to the AALs are indicated. As in Fig. 1, blue corresponds to the historical period and red to the end of this century.

It is important to recognize that statistics like those shown in the two figures are only examples of quantities that are of interest to risk assessors. With large numbers of synthetic tropical cyclone events, it is possible to estimate a wide variety of quantities that may be of interest but not calculable from limited historical data. For example, one can create a large number of realizations (say, 1,000) of 100-year time series of total annual losses in a changing climate by randomly drawing from each year's set of synthetic events, according to the average annual frequency for that year. From this, it is possible to calculate the probability of business failure, considering, for example, the random and climate-forced (e.g. ENSO-related) clustering of events. This would be a desirable statistic even in a stationary climate.

5. Summary

Historical records are too short to make accurate assessments of the long-term risk of most natural hazards, and climate change renders obsolete such assessments of weather-related hazards. In the case of tropical cyclones, climate models are too coarse to use directly to assess tropical cyclone risk, even though many research groups have done just that. Downscaling is perhaps the only viable option at this point, but suffers from the absence of two-way interaction, neglecting the possible feedback of tropical cyclones on climate. Those acquainted with tropical cyclone physics and modeling can make important contributions to social welfare by learning to convert the hazard risk into social risk and developing better ways of communicating the social risk. When that risk is effectively communicated to populations, both directly and through taxes and insurance premiums, citizens can make more informed judgements about climate action.

References

Bates, P. D., and Coauthors, 2021: Combined modelling of US fluvial, pluvial and coastal flood hazard under current and future climates. *Water Resour. Res.*, **n/a**, e2020WR028673, https://doi.org/10.1029/2020WR028673.

Danso, D. K., C. M. Patricola, and E. Bercos-Hickey, 2022: Influence of African easterly wave suppression on Atlantic tropical cyclone activity in a convection-permitting model. *Geophys. Res. Lett.*, **49**, e2022GL100590, https://doi.org/10.1029/2022GL100590.

Emanuel, K., 2022: Tropical Cyclone Seeds, Transition Probabilities, and Genesis. *J. Clim.*, **35**, 3557–3566, https://doi.org/10.1175/JCLI-D-21-0922.1.

Emanuel, K., and E. Rappaport, 2000: Forecast skill of a simplified hurricane intensity prediction model. Preprints of the 24th Conf. Hurricanes and Trop. Meteor., Ft. Lauderdale, FL, Amer. Meteor. Soc., Boston, 236–237.

——, C. DesAutels, C. Holloway, and R. Korty, 2004: Environmental control of tropical cyclone intensity. *J Atmos Sci*, **61**, 843–858.

——, R. Sundararajan, and J. Williams, 2008: Hurricanes and global warming: Results from downscaling IPCC AR4 simulations. *Bull Amer Meteor Soc*, **89**, 347–367.

Emanuel, K., F. Fondriest, and J. Kossin, 2012: Potential Economic Value of Seasonal Hurricane Forecasts. *Weather Clim. Soc.*, **4**, 110–117, https://doi.org/10.1175/wcas-d-11-00017.1.

Feldmann, M., K. Emanuel, L. Zhu, and U. Lohmann, 2019: Estimation of Atlantic Tropical Cyclone Rainfall Frequency in the United States. *J. Appl. Meteorol. Climatol.*, **58**, 1853–1866, https://doi.org/10.1175/jamc-d-19-0011.1.

Knutson, T., and Coauthors, 2019: Tropical Cyclones and Climate Change Assessment: Part I: Detection and Attribution. *Bull. Am. Meteorol. Soc.*, **100**, 1987–2007, https://doi.org/10.1175/bams-d-18-0189.1.

——, and Coauthors, 2020: Tropical Cyclones and Climate Change Assessment: Part II: Projected Response to Anthropogenic Warming. *Bull. Am. Meteorol. Soc.*, **101**, E303–E322, https://doi.org/10.1175/bams-d-18-0194.1.

Lin, N., K. A. Emanuel, J. A. Smith, and E. D.-:10. 1029/2009JD013630 Vanmarcke, 2010: Risk assessment of hurricane storm surge for New York City. *J Geophys Res*, **115**.

Patricola, C. M., R. Saravanan, and P. D.-:10. 1002/2017GL076081 Chang, 2018: The response of Atlantic tropical cyclones to suppression of African easterly waves. *Geophys. Res. Lett.*, **45**, 471–479.

Rotunno, R., Y. Chen, W. Wang, C. Davis, J. Dudhia, and C. L. Holland, 2009: Large-eddy simulation of an idealized tropical cyclone. *Bull Amer Meteor Soc*, **90**, 1783–1788.

The roles of wind-induced surface heat exchange in secondary eyewall formation, rapid intensification and size of tropical cyclones

Chun-Chieh Wu
Department of Atmospheric Sciences, National Taiwan

cwu@as.ntu.edu.tw

Abstract

In this lecture, we plan to review a series of recent studies examining the roles of surface heat fluxes, particularly in relation to the wind-induced surface heat exchange (WISHE; Emanuel 1989) mechanism, in (i) secondary eyewall formation (SEF), (ii) rapid intensification (RI), and (iii) size of tropical cyclones (TCs). Numerical experiments, in which the surface wind used for the surface flux calculations is capped at varying magnitudes and at different radial intervals, have been performed to investigate the role of WISHE in TC structure and intensity change.

(i) The Dynamics of SEF will first be reviewed through the works of Wu et al. (2012), Huang et al. (2012), and Huang et al. (2018), followed by major findings from Cheng and Wu (2018). To examine the sensitivity of SEF to the WISHE mechanism, the surface wind used for the calculation of surface heat fluxes is capped at several designated values and at different radial intervals. When the heat fluxes are moderately suppressed around and outside the SEF region observed in the control experiment, sensitivity experiments show that the formation of the outer eyewall is delayed, and the intensity of both eyewalls is weaker. When the heat fluxes are strongly suppressed in the same region, SEF does not occur. In contrast, suppressing the surface heat fluxes in the storm's inner-core region has limited effect on the evolution of the outer eyewall. This study provides important physical insight into SEF, indicating that the WISHE mechanism plays a crucial role in SEF.

(ii) The study of RI by Chang and Wu (2017) will be reviewed, and then results from Cheng and Wu 2020 will be discussed. Sensitivity experiments with capped surface fluxes and reduced WISHE exhibit delayed RI and weaker peak intensity, while WISHE could affect the evolutions of TC both before and after the onset of RI. Before RI, more WISHE leads to faster increase of equivalent potential temperature in the

lower levels, resulting in the eruption and the axisymmetrization of the convection (especially in the lower levels). In addition, TCs in experiments with more WISHE reach a certain intensity level earlier, before the onset of RI. During the RI period, more surface heat fluxes cause more efficient intensification in a TC, leading to a stronger peak intensity, a more significant and deeper warm core in the TC center, and the axisymmetrization of convection in the higher levels. In both stages, different levels of WISHE alter the thermodynamic environment and convective-scale processes. With WISHE, a consequent development in the convective activity is identified, resulting in a stronger secondary circulation and increased diabatic heating. Within the inner-core region, deeper inflow increases the transport of angular momentum from the outer radii, leading to faster spin-up of the tangential circulation. In all, the important role of the WISHE feedback in RI, both during the pre-RI stage and during the RI period, is highlighted. In the case of Typhoon Megi (2010), a weaker WISHE effect delays the RI onset time, and the simulated storm therefore has a weaker peak intensity. A stronger WISHE effect leads to a faster increase of low-level equivalent potential temperature and thus higher convective instability, resulting in more frequent and stronger convective activity and faster TC intensification rates. The simulated storm can therefore reach a stronger peak intensity, and establish a stronger and deeper TC warm core.

In a separate study (Peng and Wu 2020), the RI of Typhoon Soudelor (2015) was simulated using a full-physics model. To investigate how the outer-core surface heat fluxes affect TC structure and RI processes, a suite of numerical experiments were performed by suppressing surface heat fluxes between various radii. It was found that a TC would become much weaker when the surface heat fluxes are suppressed outside the radius of 60 or 90 km (the radius of maximum surface wind in the control experiment at the onset of RI is roughly 60 km). However, interestingly, the TC would experience stronger RI when the surface heat fluxes are suppressed outside the radius of 150 km. For those sensitivity experiments with capped surface heat fluxes, the members with greater intensification rate show stronger inner-core mid- to upper-level updrafts and higher heating efficiency prior to the RI periods. Although the outer-core surface heat fluxes in these members are suppressed, the inner-core winds become stronger and extract more ocean energy from the inner core. Greater outer-core low-level stability in these members results in aggregation of deep convection and subsequent generation and concentration of potential vorticity inside the inner core, thus confining the strongest winds therein. The above-mentioned findings are also

supported by partial-correlation analyses, which reveal the positive correlation between the inner-core convection and subsequent 6-h intensity change, and the competition between the inner-core and outer-core convections (i.e., eyewall and outer rainbands).

In all, suppression of the WISHE mechanism within the radial interval from 1 to 2.5 times the inner-core size effectively hinders the RI in the case of a simulated Typhoon Soudelor (2015). In contrast, suppression of the WISHE process outside of this radial interval slightly facilitates RI due to the suppressed/concentrated convective activities in the outer-core/inner-core region.

(iii) Shen et al. (2021) attempted to understand how surface heat fluxes in different storm regions affect TC size. The Advanced Research Weather Research and Forecasting (ARW-WRF) model (version 3.5.1) was used to simulate Typhoon Megi (2016). A series of numerical experiments were carried out, including a control simulation and several sensitivity experiments with surface heat fluxes suppressed in different TC regions (to mimic the reduction of the WISHE feedback in the inner and/or outer core). The results showed that with surface heat fluxes suppressed in the entire domain, the TC tends to be smaller. Meanwhile, the TC size is more sensitive to the surface heat flux change in the outer core than to that in the inner core. Suppressing surface heat fluxes can weaken the rainbands around the suppressed area, which in turn slows down the secondary circulation. When the surface heat flux is suppressed in the inner-core region, the weakening of the secondary circulation associated with the diminished inner rainbands is limited to the inner core region, and only slightly affects the absolute angular momentum import from the outer region, thus having negligible impact on TC size. However, suppression of surface heat fluxes in the outer-core region leads to less active outer rainbands and a more substantial weakening of the secondary circulation. This results in less absolute momentum import from the outer region, and in turn, a smaller TC.

In all, while suppression of the WISHE mechanism in the whole outer-core region constricts the size of Typhoon Megi (2016), the same degree of suppression on WISHE in a narrow ring region (3 - 4 *RMW, radius of maximum wind) results in a lager TC. In the former case, suppression of surface heat fluxes in the outer-core region leads to less active outer rainbands and a more substantial weakening of secondary circulation, resulting in less import of absolute momentum and in turn a smaller TC. In the latter case, the TC expansion is attributed to enhanced convection near the outer edge of the ring, where the boundary layer inflow decelerates and the low-level convergence.

References:

Chang, C.-C., and C.-C. Wu*, 2017: On the processes leading to the rapid intensification of Typhoon Megi (2010). *J. Atmos. Sci.,* **74**, 1169-1200. doi: 10.1175/JAS-D-16-0075.1

Cheng, C.-J., and C.-C. Wu*, 2018: The role of WISHE in secondary eyewall formation. *J. Atmos. Sci.,* **75**, 3823-3841. doi: 10.1175/JAS-D-17-0236.1

Cheng, C.-J., and C.-C. Wu*, 2020: The role of WISHE in the rapid intensification of tropical cyclones. *J. Atmos. Sci.*, **77**, 3139-3160. doi: https://doi.org/10.1175/JAS-D-20-0006.1

Chih, C.-H., and C.-C. Wu*, 2020: Exploratory analysis of upper ocean heat content and sea surface temperature underlying tropical cyclone rapid intensification in the western north Pacific. *J. Climate*, **33**, 1031-1050. doi: 10.1175/JCLI-D-19-0305.1

Emanuel, K.A., 1989: The finite-amplitude nature of tropical cyclogenesis. *J. Atmos. Sci.*, **46**, 3431-3456, doi: 10.1175/1520-0469(1989)046<3431:TFANOT>2.0.CO;2.

Huang, Y.-H., M. T. Montgomery, and C.-C. Wu*, 2012: Concentric eyewall formation in Typhoon Sinlaku (2008) – Part II: Axisymmetric dynamical processes. *J. Atmos. Sci.,* **69**, 662-674. doi: 10.1175/JAS-D-11-0114.1

Huang, Y.-H., C.-C. Wu*, and M. T. Montgomery, 2018: Concentric eyewall formation in Typhoon Sinlaku (2008). Part III: Horizontal momentum budget analyses. *J. Atmos. Sci.,* **75**, 3541-3563. doi: 10.1175/JAS-D-18-0037.1

Peng, C.-H., and C.-C. Wu*, 2020: The impact of outer-core surface heat fluxes on the convective activities and rapid intensification of tropical cyclones. *J. Atmos. Sci.,* **77**, 3907-3927. doi: https://doi.org/10.1175/JAS-D-19-0348.1

Shen, L.-Z., C.-C. Wu*, and F. Judt, 2021: The role of surface heat fluxes on the size of Typhoon Megi (2016). *J. Atmos. Sci.,* **78,** 1075-1093. doi: https://doi.org/10.1175/JAS-D-20-0141.1

Wu, C.-C.*, Y.-H. Huang, and G.-Y. Lien, 2012: Concentric eyewall formation in Typhoon Sinlaku (2008) – Part I: Assimilation of T-PARC data based on the Ensemble Kalman Filter (EnKF). *Mon. Wea. Rev.,* **140**, 506-527. doi: 10.1175/MWR-D-11-00057.1

A Unified Time-Dependent Theory of Tropical Cyclone Intensification and Its applications: Current Status and Future Directions

Yuqing Wang
Department of Atmospheric Sciences and International Pacific Research center, School of Ocean and Earth Science and Technology, University of Hawaii at Manoa, Honolulu,
yuqing@hawaii.edu

Upon the genesis of a tropical depression under favorable environmental conditions, such as high sea surface temperature (SST) and high heat content in the uppermost ocean layer, and weak vertical wind shear, the cyclonic low-pressure system may develop into a tropical cyclone (TC). In the absence of detrimental environmental effects, a TC often experiences a phase of rapid intensification associated with an increase in near-surface maximum wind speed of more than 15 m s^{-1} per day, before it reaches its maximum intensity. Over the past five decades or so, many efforts have been devoted to conceptualizing the physical mechanisms that are responsible for TC intensification. Each of the proposed mechanisms describes a kind of positive feedbacks and can give a qualitative explanation for TC intensification processes to some extent. However, none of the concepts can provide a quantitative measure of the intensification rate of a TC.

Unlike the maximum potential intensity (MPI), i.e., the maximum intensity a TC may reach under given favorable environmental conditions (Emanuel 1986, 1997), the TC intensification rate may depend on the intensity of the TC itself, the radial location of diabatic heating, and both the inner- and outer-core structures of the TC vortex. Although two time-dependent equations for TC intensification rate have been proposed under various assumptions in the literature (Emanuel 2012; Ozawa and Shimokawa 2015), neither of them can capture the intensity-dependent TC intensification rate in observations (Xu and Wang 2015, 2018).

A fundamental advancement in recent years has been the development of a unified time-dependent theory of TC intensification, which can capture the major features of TC intensification in both observations and full-physics model simulations (Wang et al., 2021a,b, 2022, 2023). In particular, with the introduction of environmental factors, the unified theory can be used to understand the impact of various environmental factors on TC intensity change in observations and to perform real-time TC intensity forecasts. The theory also provides a basis for understanding and evaluating impact of climate change on TC intensification. In this lecture, the current status will be given and the future directions in this line will be briefly discussed.

There are two versions in the literature: one is energetically based and the other is dynamically based. The energetically based theory considers a TC vortex as an unsteady Carnot heat engine. Namely, instead of a balance between the power generation and power dissipation for a steady-state heat engine assumed for the TC MPI (Emanuel 1997), the power generation during the intensification stage is larger than the power dissipation, the power gain will then be used to increase the kinetic energy of the TC system.

$$\int\int \rho \frac{\partial}{\partial t}\left(\frac{1}{2}\left|\vec{V}\right|^2\right) r dr dz = E \int \rho \epsilon C_k \left|\vec{V}\right| (\kappa_o^* - \kappa_a) r dr - \int \rho C_D \left|\vec{V}\right|^3 r dr, \qquad (1)$$

where a TC is assumed to be axisymmetric, r is radius, C_k, C_D are the surface exchange coefficient for enthalpy and momentum, respectively, ρ is the air density near the surface, $\left|\vec{V}\right|$ is the near-surface wind speed, κ_o^* the saturated enthalpy of the ocean surface at a

given SST (T_S), κ_a the enthalpy of the atmosphere near the surface, $\varepsilon = (T_s - T_0)/T_s$ is the thermodynamic efficiency of the heat engine with T_0 being the outflow temperature, E is the dynamical efficiency, namely the percentage of the potential energy being converted to kinetic energy (Wang et al. 2021a). Note that $|\vec{V}|$ on the rhs of Eq. (1) represents the near-surface wind speed, while that on the lhs represents wind speed in the inner-core column.

Considering the fact that the intensification of a TC is dominated by the increase in wind speed (kinetic energy) near the RMW, the integration of Eq. (1) can be approximated by

$$H\bar{\rho}\bar{V}\frac{\partial \bar{V}}{\partial \tau} = E\rho_0 \varepsilon C_k V_{max}(\kappa_o^* - \kappa_a)_{rm} - \rho_0 C_D V_{max}^3, \quad (2)$$

where H is the scale height of the inner-core column, the change with time τ means the change following the RMW, overbar means the corresponding column mean, ρ_0 the air density near the ocean surface, and V_{max} is the maximum near-surface wind speed at the RMW, namely the TC intensity by definition. Eq. (2) can be simplified to

$$\frac{\partial V_{max}}{\partial \tau} = \frac{\alpha C_D}{h}\left(EV_{mpi}^2 - V_{max}^2\right), \quad (3)$$

here $\alpha/h = \rho_0/(\bar{\rho}H\mu^2)$, with $\mu = \bar{V}/V_{max}$, the column mean total wind speed scaled by the maximum near-surface wind speed, α is introduced so that the rescaled height parameter h is equivalent to the depth of the well-mixed boundary layer in the inner core ($\sim 2000m$). We will see from the dynamically based theory below that α is similar to the reduction factor of the near-surface wind speed from the boundary layer depth-mean wind speed, which ranges between 0.7~ 0.8. The MPI (V_{mpi}) in (3) is given by

$$V_{mpi} = \sqrt{\frac{C_k}{C_D}\varepsilon(\kappa_o^* - \kappa_a)|_{r_m}}. \quad (4)$$

The dynamical efficiency E in Eq. (3) needs to be determined to make the time-dependent theory closed. Since the steady-state TC intensity should be equal to its MPI given all favorable environmental conditions, the dynamical efficiency E should be 1.0 for a steady-state solution. However, when the TC is very weak, the Rossby radius of deformation is large and the dynamical efficiency of the heat engine much be very low as implied from the balanced dynamics (Schubert and Hack 1982). As a result, $E \to 0, as\ V_{max} \to 0$. Based on calibration of results from both idealized full-physics numerical simulations and TC best-track data, E can be expressed as a function of relative intensity (Wang et al., 2021b) given below

$$E = \left(V_{max}/V_{mpi}\right)^{3/2}, \quad (5)$$

The above energetically based time-dependent equation of TC intensification can also be obtained based on dynamics (Wang et al., 2021b). In a slab boundary layer, the tangential wind and entropy budget equations for an axisymmetric TC vortex can be written as

$$\frac{\partial V_b}{\partial t} + u_b\frac{\partial M_b}{r\partial r} = -\frac{C_D}{h}|\vec{V}|V_T, \quad (6)$$

$$\frac{\partial s_b}{\partial t} + u_b\frac{\partial s_b}{\partial r} = \frac{C_k}{h}|\vec{V}|(s_0^* - s_b), \quad (7)$$

where M_b, V_b and u_b are the depth-averaged AAM, tangential, and radial wind velocities in the boundary layer, which has a depth of h, $|\vec{V}|$ and V_T are the total wind speed and the tangential wind speed near the sea surface, respectively, s_0^* and s_b are the saturated entropy at the underlying SST and the well-mixed air entropy in the slab boundary layer. Note that the horizontal diffusions of both tangential wind and entropy are neglected although they may be important across the eyewall in strong TCs.

Since the TC intensification is defined as the rate of change in the near-surface wind

speed following the RMW (r_m), all terms in Eqs. (6) and (7) should be evaluated following the RMW. Because of the large radial entropy gradient and strong inflow and the highly elevated entropy flux across the RMW, the local change in entropy near the RMW is relatively small. Therefore, a thermodynamic quasi-equilibrium near the RMW can be assumed, and thus Eq. (7) can be approximated as

$$u_b \frac{\partial s_b}{\partial r}|_{rm} = \frac{C_k}{h}|\vec{V}|(s_0^* - s_b)|_{rm}. \quad (8)$$

Combining Eqs. (6) and (8) gives

$$h\frac{\partial V_b}{\partial \tau} = -\frac{1}{r_m}\frac{\partial M_b}{\partial r}C_k|\vec{V}|(s_0^* - s_b)/\frac{\partial s_b}{\partial r} - C_D|V|V_T. \quad (9)$$

Note that in Eq. (9), τ is used instead of t because the budget and all variables are now evaluated following the RMW. Since the total wind speed at the RMW is close to the tangential wind speed, we can assume $|\vec{V}| \approx V_T = V_{max}$. We further assume $V_{max} = \alpha V_{b,m}$, where α is the reduction factor from the depth-averaged boundary layer wind speed to the near-surface wind speed at the RMW, which is roughly between 0.7~0.8 based on observations. With these approximations, Eq. (8) can be rewritten as

$$\frac{\partial V_{max}}{\partial \tau} = \frac{\alpha}{h}\left[-\frac{1}{r_m}\frac{\partial M}{\partial s}\Big|_{b,r_m} C_k V_{max}(s_0^* - s_b)|_{r_m} - C_D V_{max}^2\right]. \quad (10)$$

The continuity at the top of the boundary layer requires $\frac{\partial M}{\partial s}\Big|_{b,r_m} \cong \frac{\partial M}{\partial s}\Big|_{h,r_m}$. Therefore, Eq. (10) can be closed if $\frac{\partial M}{\partial s}\Big|_{h,r_m}$ can be determined. Following Emanuel (1986), we assume that the TC vortex in the free atmosphere above the boundary layer is axisymmetric and in thermal wind balance, If both s and M are assumed to be conserved along streamlines, the s and M surfaces are congruent, or equivalently the state of moist-neutral eyewall ascent is along M surfaces (Emanuel, 1986), we have

$$\frac{1}{r^3}\left(\frac{\partial r}{\partial p}\right)_M = \frac{1}{2M}\frac{\partial s}{\partial M}\left(\frac{\partial T}{\partial p}\right)_s, \quad (11)$$

If we integrate Eq. (12) along a trajectory of moist-neutral ascent (constant M and s surface) starting from the RMW at the top of the boundary layer (r_m, h) to the point at a large radius (r_0) in the upper tropospheric outflow where the trajectory becomes essentially horizontal and tangential wind becomes zero, we can have (Bryan and Rotunno 2009b)

$$\frac{dM}{ds}\Big|_{h,r_m} = -\frac{T_b - T_0}{M_{h,r_m}\left(\frac{1}{r_m^2} - \frac{1}{r_0^2}\right)}, \quad (12)$$

where T_b is air temperature at (r_m, h), T_0 is the air temperature at the outer radius r_0 in the outflow. Note that although the assumption of moist-neutral convection in the eyewall is a good approximation for a strong TC, this is often not satisfied during the TC intensification stage. Namely, the M and s surfaces would not be congruent but intersect, especially (Peng et al., 2018). Therefore, an *ad hoc* parameter A can be introduced into Eq. (12), thus we have (Wang et al., 2021b)

$$\frac{\partial M}{\partial s}\Big|_{b,r_m} \cong \frac{\partial M}{\partial s}\Big|_{h,r_m} = -A\frac{T_b - T_0}{M_{h,r_m}\left(\frac{1}{r_m^2} - \frac{1}{r_0^2}\right)}, \quad (13)$$

where A denotes the extent to which the M surface is parallel to the s surface, which should satisfy $0 \le A \le 1$ considering $(\partial M/\partial s)_{h,r_m} \le 0$. A should be close to 1.0 when the eyewall convection reaches a nearly moist-neutral state with the M and s surfaces being almost congruent as in Eq. (12), while it is close to zero in the early incipient stage when V_{max} is close to zero and the M and s surfaces are nearly orthogonal (Peng et al., 2018). Substituting Eq. (13) into Eq. (10) and using the approximations of ($T_b \approx T_s$), $V_{b,rm} \approx V_{max}$, and $(k_0^* - k_B) \approx T_s(s_0^* - s_b)$, Eq. (10) can be simplieid to

$$\frac{\partial V_{max}}{\partial \tau} = \frac{\alpha C_D}{h}\left(AV_{mpi}^2 - V_{max}^2\right), \tag{14}$$

where again V_{mpi} is the MPI defined in Eq. (4).

Mathematically, Eq. (14) is identical to Eq. (3) except that E is replaced by A. Although the parameter A introduced in the dynamically based theory and the dynamical efficiency E in the energetically based theory have different physical meanings, they both are nondimensional and thus share the same dependence on relative intensity as given in Eq. (5) as demonstrated by Wang et al. (2021b) and Xu and Wang (2022). Since the *ad hoc* parameter A measures the extent to which the M and s surface are confluent in the eyewall updraft, it is termed the ventilation parameter (Wang et al., 2021b). Namely a smaller A indicates a larger intersection angle between M and s surfaces. In this case, less potential energy is converted to kinetic energy, with a smaller dynamical efficiency. Substituting Eq. (5) into either Eq. (3) or Eq. (15), we can have

$$\frac{\partial V_m}{\partial \tau} = \frac{\alpha C_D}{h} V_{mpi}^2 \left[\left(\frac{V_m}{V_{mpi}}\right)^{3/2} - \left(\frac{V_m}{V_{mpi}}\right)^2\right], \tag{15}$$

Eq. (15) was derived both energetically and dynamically. The first term on the rhs of Eq. (15) is the intensification potential while the second term is the weakening tendency due to surface friction.

Note that the time-dependent theory above was derived under idealized environmental conditions, and thus it reflects the potential intensification rate (PIR) a TC vortex can reach with a given favorable thermodynamic environment. The theory can reproduce well the intensity evolution of TCs in idealized, full-physics model simulations (Wang et al., 2021b) and capture the observed PIR of real TCs (Xu and Wang, 2022). The theory has been extended to include the contribution of dissipative heating and the thermodynamic expansion of the boundary layer inflow to TC intensification (Wang et al., 2022; 2023). In general, both effects increase with increasing TC intensity.

Although the theory was obtained for a TC in a quiescent environment, it can be extended to include the detrimental environmental dynamical effects by introducing an environmental dynamical efficiency or environmental ventilation parameter (Wang et al., 2021b). In this case, the first term in Eq. (15) should be multiplied by such an efficiency or ventilation parameter (B), which is always less than 1.0. In this case, Eq. (15) can be revised to

$$\frac{\partial V_{max}}{\partial \tau} = \frac{\alpha C_D}{h} V_{mpi}^2 \left[B\left(\frac{V_{max}}{V_{mpi}}\right)^{3/2} - \left(\frac{V_{max}}{V_{mpi}}\right)^2\right]. \tag{16}$$

Physically, the parameter B can be considered as the collective detrimental effect of environmental factors, such as vertical wind shear, that ventilate the eyewall entropy both in and above the boundary layer, reducing the extent to which the M and s surfaces are confluent and thus the intensification rate of the TC. If B is parameterized using environmental factors and calibrated based on best-track TC data, Eq. (16) can be potentially used for operational TC intensity prediction.

In addition, since many studies have projected an increase in MPI in a warmer future climate, Eq. (16) implies that TCs in a warmer climate may intensify more rapidly. For example, a 5% increase in MPI may lead to a 10.25% increase in TC PIR. Since rapid intensification is still a challenge in current operational forecasts, the increasing intensification rate may make the TC intensity more difficult to predict in the future under global warming as also discussed by Emanuel (2017).

References

Bryan, G. H, Rotunno, R., 2009b. The maximum intensity of tropical cyclones in axisymmetric numerical model simulations. *Mon. Wea. Rev*., **137**, 1770–1789.

Emanuel, K. A., 1986. An air-sea interaction theory for tropical cyclones. Part I: Steady state maintenance. *J. Atmos. Sci.*, **43**, 585–604.

Emanuel, K.A., 1997. Some aspects of hurricane inner-core dynamics and energetics. *J. Atmos. Sci.*, **54**, 1014–1026.

Emanuel, K. A., 2017. Will global warming make hurricane forecasting more difficult? *Bull. Amer. Meteor. Soc.*, **98**, 495–501.

Emanuel, K. A., 2012: Self-stratification of tropical cyclone outflow: Part II: Implications to storm intensification. *J. Atmos. Sci.*, **69**, 988–996,

Ozawa, H., and S. Shimokawa, 2015: Thermodynamics of a tropical cyclone: generation and dissipation of mechanical energy in a self-driven convection system. *Tellus A*, **67**, 24216.

Peng, K., R. Rotunno, and G. H. Bryan, 2018: Evaluation of a time- dependent model for the intensification of tropical cyclones. *J. Atmos. Sci.*, **75**, 2125–2138.

Schubert, W. H., Hack, J. J., 1982. Inertial stability and tropical cyclone development. *J. Atmos. Sci.*, **39**, 1687–1697.

Wang, Y., Li, Y.-L., Xu, J., 2021a. A new time-dependent theory of tropical cyclone intensification. *J. Atmos. Sci*., **78**, 3855–3865.

Wang, Y., Li, Y.-L., Xu, J., Tan, Z.-M., Lin, Y.-L., 2021b. The intensity-dependence of tropical cyclone intensification rate in a simplified energetically based dynamical system model. *J. Atmos. Sci*., **78**, 2033–2045.

Wang, Y., J. Xu, and Z.-M. Tan, 2022: Contribution of dissipative heating to the intensity-dependence of tropical cyclone intensification. *J. Atmos. Sci.*, **79**, 2169–2180.

Wang, Y., Z.-M. Tan, and Y.-L. Li, 2023: Some refinements to the most recent simple time-dependent theory of tropical cyclone intensification and sensitivity. *J. Atmos. Sci.*, **79**, 321–335.

Xu, J., and Y. Wang, 2015: A statistical analysis on the dependence of tropical cyclone intensification rate on the storm intensity and size in the North Atlantic. *Wea. Forecasting*, **30**, 692–701.

Xu, J., and Y. Wang, 2018: Dependence of tropical cyclone intensification rate on sea surface temperature, storm intensity and size in the western North Pacific. *Wea. Forecasting*, **33**, 523–537.

Xu, J., Wang, Y., 2022. Potential intensification rate of tropical cyclones in a simplified energetically based dynamical system model: An observational analysis. *J. Atmos. Sci.*, **79**, 1045–1055.